Tellus (1993), *45A*, 99–113

Numerical experiments on a possible mechanism of cyclogenesis in the Antarctic region

By MAURIZIO FANTINI and ANDREA BUZZI, *FISBAT-CNR, c/o Dept. of Physics, via Irnerio 46, I 40126, Bologna, Italy*

(Manuscript received 8 May 1992; in final form 25 September 1992)

ABSTRACT

Polar lows are observed to form in the circum-Antarctic ocean, where strong meridional thermal contrast in the atmosphere is normally associated with large heat fluxes from the sea. In the present study, using a two-dimensional non-hydrostatic model, we examine the growing stage of disturbances that bear many characteristics in common with observed polar lows, as, for example, warm mesoscale updrafts where the latent heat is released. We show here that such growing disturbances do not depend, for their structure and scale, on the initial condition chosen. Growth rates are considerably larger than those of modes in the absence of surface heat fluxes, and may be sustained for several days.

1. Introduction

Observational evidence of mesoscale (100–1000 km) vortices in the atmosphere around Antarctica was presented, among others, by Carleton and Carpenter (1989), Bromwich (1989), Heinemann (1990) and Fitch and Carleton (1992). Aside from the small horizontal scale, the dominant features are their occurrence over the ocean and the evidence of deep convection. Among the various processes that have been suggested to account for those cyclones, we are interested here in the combined action of baroclinicity and heat fluxes from the ocean. Our view is based on the work by Emanuel and Rotunno (1989) (hereafter referred to as ER) which showed that the difference of temperature and/or moisture content between the cold air and the relatively warm water is a source of energy sufficient to maintain an organized convective system against frictional dissipation. Such a system has many features in common with a tropical cyclone as modeled by the same authors (Rotunno and Emanuel, 1987). ER proved this point by running a primitive-equation numerical model in conditions similar to those obtained in the Arctic, but with no background baroclinicity. The circulation that develops collects sensible and latent heat fed by diffusive fluxes from the sea into the boundary layer and transports it towards the center of the vortex, where the air is lifted and latent heat released, contributing to the kinetic energy of the storm. While this mechanism was shown to be efficient for polar lows in the mature stage by ER (and for tropical storms in the previous (Emanuel, 1986; Rotunno and Emanuel, 1987), the numerical simulations had to be initialized with a vortex of the appropriate magnitude and strength. The question as to what provides this initial perturbation in the real world was left open, although baroclinic instability was suggested as an obvious candidate.

The relevance of baroclinicity and baroclinic instability for the initiation of polar lows in the Arctic environment has been stressed by many authors (e.g., Mansfield, 1974; Sardie and Warner, 1983; Rasmussen, 1985; Wiin-Nielsen, 1989; Rasmussen et al., 1992). This possibility is even stronger in the Antarctic environment, as can be inferred from the annual averages of zonal wind and potential temperature shown in Hoskins et al. (1989) and from the study of Fitch and Carleton (1992). It is evident from those climatological analyses that the circum-Antarctic region is characterized by local maxima of both low-level heating rate and baroclinicity.

The role of the initial condition for polar low development would be to set up the circulation described above and maintain it up to the point where it can sustain itself by means of latent heat release, fed by the heat fluxes from the sea. In the same climatological analyses of Hoskins et al. (1989) it is evident that the circum-Antarctic ocean is also characterized by a maximum of diabatic heating, due to the combination of strong surface winds and a sharp temperature contrast between air and sea. In practice, a baroclinic low would provide the large scale collection of heat by the geostrophic wind and the convergence toward the center by means of the cross-isobar flow.

In the paper by Heinemann (1990), the possibility was suggested that katabatic winds from the continent may cause a zone of high convergence over the ocean. This occurrence could also provide a favourable initial condition for the ER mechanism but we were unable to reproduce it within this model. The present work concerns the stages of development of a "polar low" in the sense of ER, where, we wish to show, the presence of environmental baroclinicity can provide the finite amplitude initial condition needed for the organization of the heat fluxes. We are not concerned with the fully mature stage or the maintenance of the steady state, whose study is precluded by geometrical considerations.

In order to obtain a simple representation of baroclinic instability, we use a two-dimensional model in Cartesian coordinates. All the phenomena obtained in the model are then slab-symmetric by definition, including the organized convective systems which we will refer to, for simplicity, as "2D polar lows" or even "2D hurricanes", but which lack all the axisymmetric structure of the 3-D world. With the term "2D hurricane" structure we refer to that particular flow organization which emerges, in our solution, during the convective stage that follows the baroclinic stage, in the cases where surface fluxes are active. We also note, in this regard, that polar lows have been divided into two main categories, depending on their shape: comma cloud lows and spiral lows. Both types have been observed in the Arctic (Rasmussen et al., 1992) as well as in the Antarctic region. It is clear that the comma cloud type lacks the axial symmetry of the spiral type. The former is then more likely to form in a baroclinic environment and is, therefore, a better referent for our study.

2. Model description

The model is a 2-D version of the primitive-equation non-hydrostatic model of Klemp and Wilhelmson (1978), with simplified thermodynamics. Neither liquid water nor ice are considered. An equation for the mixing ratio of water vapour q_v is integrated and, when saturation is reached, potential temperature θ and q_v are recalculated according to

$$\Delta_C \theta = -\frac{L}{c_p \bar{\Pi}} \Delta_C q_v,$$

$$q_v + \Delta_C q_v = q_v^s(\theta + \Delta_C \theta, \bar{\Pi})$$

(where Π is the Exner function, and q_v^s the saturation mixing ratio), but all the condensed water is lost.

The model integrates the equations of motion on a rectangular domain in the (x, z) plane and periodic boundary conditions are applied in the x-direction. We can consider different wavelengths of baroclinic waves by changing the size of the domain. Only the vertical velocity w is known at top and bottom boundaries, and the condition $w = 0$ is imposed there. The model has an internal dissipation with a mixing length of 50 km in the horizontal direction and of 200 m in the vertical, the vertical mixing being active only when the local Richardson number is below 1. The relatively high value of the horizontal mixing length l_H is responsible for a general smoothing of the dynamical fields. Sensitivity experiments with lower values of l_H, which we will not show here, give the same general results with an higher level of grid-scale noise, and somewhat higher growth rates. We use a fixed number of grid points: 15 in the vertical, corresponding to a 1-km vertical resolution; and 100 in the horizontal. When we change the horizontal size of the domain to examine different wavelengths we also change horizontal resolution. The two experiments we will present in Section 3 have been run with horizontal resolutions of 20 and 15 km, respectively.

To adapt the model to polar environment we have taken the Coriolis parameter corresponding to a latitude of 65°, i.e., $f_o = 1.3 \cdot 10^{-4}\ s^{-1}$, but we are not using the minus sign of the Southern Hemisphere. We have designed an idealized thermodynamic profile, shown in Fig. 1, consisting

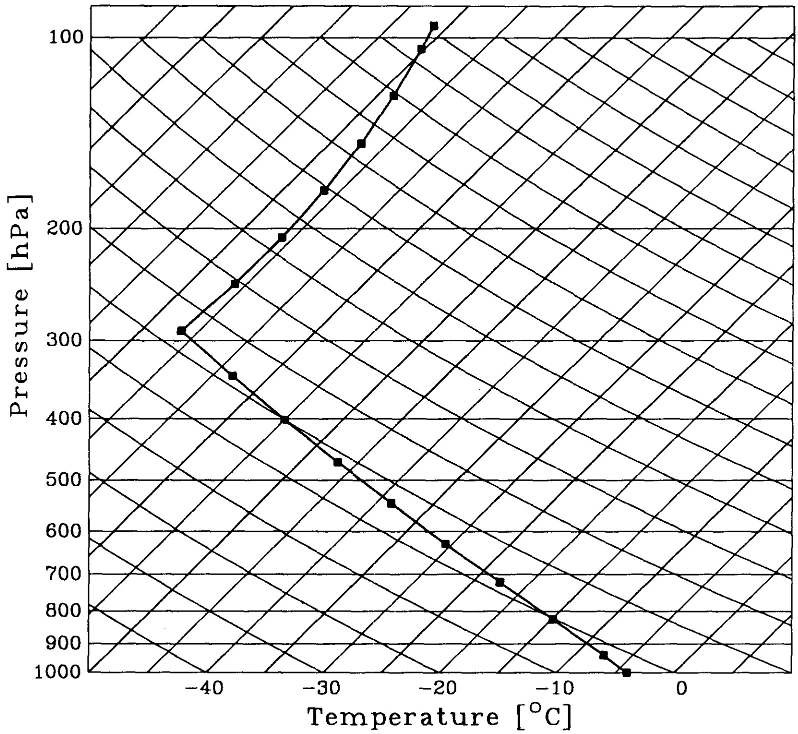

Fig. 1. Potential temperature profile used for all the experiments shown, in a Skew T − log p diagram.

of a uniformly stable troposphere, with a lapse rate typical of polar low environment. The tropopause height is set to a climatological value for Antarctica (e.g., Hoskins et al., 1989). The model's stratosphere contains, in its upper half, a sponge layer to absorb gravity waves. The graphs in the next section will show only the part of the domain below the sponge layer.

The meridional advection of thermodynamic quantities, necessary to model a baroclinic environment, is treated by using a constant meridional gradient of potential temperature $\bar{\theta}_y$, which implies by geostrophic balance a uniform vertical shear of the zonal wind $\bar{u}_z$. For the reasons explained in detail in Fantini (1993) we also impose a y-independent relative humidity H and calculate the meridional advection of mixing ratio as

$$v\frac{\partial q_v}{\partial y} = v\left(\frac{q_v(y_o) - q_v^s(y_o - v\,\Delta t)\cdot H}{v\,\Delta t}\right), \qquad (1)$$

where y_o is the meridional coordinate of the model's plane, and the derivative is calculated upstream over the distance travelled by an air parcel during a time step. The relative humidity $H(x, z, t)$ is determined by the dynamics on the $x-z$ plane, and it is calculated at every time step at each grid point. It is then assumed that this quantity does not change in the meridional direction, so that the y-derivative of water vapour mixing ratio can be calculated as in (1) above. All quantities on the right-hand side of (1) are known, because the saturation mixing ratio q_v^s is a known function of θ and Π, whose meridional variation is imposed initially for the base state and is zero for the perturbations.

This whole procedure is weakly inconsistent with slab-symmetry, in that it would generate by condensation θ perturbations that are not y-independent. In other words, if we had a fully 3-D model and initialized it with a y-independent relative humidity, the evolution of the model would generate a meridional structure in all the dynamical variables due to the non-linear nature of the saturation law. We can however evaluate the magnitude of the errors we introduce in the course of the experiments, the largest of which is due to the different amounts of latent heat released at different y locations. Taking y_o to be the meridional coordinate of the plane of the model, the quantity

$$\theta_{\mathrm{err}} = \frac{L}{c_p}\left[\frac{\Delta_C q_v(y_o)}{\bar{\Pi}(y_o)} - \frac{\Delta_C q_v(y_o - v\,\Delta t)}{\bar{\Pi}(y_o - v\,\Delta t)}\right]$$

gives the error in θ perturbation introduced over one time step. We monitor the accumulation of these errors throughout the integration. For all the experiments presented in the next section this quantity is at least an order of magnitude smaller than the dynamical θ perturbation, reaching values of the order of a tenth of a degree at the end of the integrations.

The momentum drag and heat fluxes at the surface are written

$$F_{[u,v]} = c_D \sqrt{u'^2 + v^2}\,[u', v],$$
$$F_{[\theta, q_v]} = c_E \sqrt{u'^2 + v^2}\,([\theta_{\mathrm{sea}}, q_{v,\mathrm{sea}}] - [\theta, q_v]),$$

with wind-dependent drag coefficients

$$c_D = c_E = 1.1 \cdot 10^{-3} + 4 \cdot 10^{-5} \sqrt{u'^2 + v^2}.$$

The quantities with subscript $_{\mathrm{sea}}$ refer to air in contact with the sea surface. The model variables u', v, θ, q_v in the above expressions are at the lowest level. u' is the zonal perturbation velocity component, defined as the total zonal velocity minus the basic zonal wind $\bar{u}$. This is equivalent to assuming $\bar{u} = 0$ at the lower boundary. However, in the following experiments we choose a mean basic zonal wind in such a way that our reference frame moves approximately with the perturbation, so that the apparent basic zonal wind at the ground does not vanish. The heat flux is driven by imposing a sea surface warmer than the air above it. To maintain the y-independence of the perturbations the imposed air-sea temperature difference $\Delta\theta$ is a constant. In our baroclinic environment this implies that the SST has a meridional gradient as well, which parallels the meridional gradient of surface air temperature.

We initialize the experiments with a meridional wind perturbation in the form of a sine of the horizontal coordinate, with a $\pi/4$ westward phase tilt between the bottom and top boundaries. The other fields are then adjusted geostrophically. This perturbation would project highly on the most unstable dry baroclinic wave, while for the moist short-wave cases we are considering, it is at any rate a growing baroclinic perturbation.

A similar work, but with a different thermodynamics, was presented in Fantini (1990), although the main interest there was on mid-latitude explosive developments. The procedure here described for the meridional advection of moisture allows us to use realistic thermodynamics on the (x, z) plane, the difference from previous work being of some relevance in the case of a rather cold environment. A more extensive discussion of these points are to be found in Fantini (1993).

Finally we note that the re-evaporation of liquid water had an inhibiting effect on the ER mechanism, and that is missing in the present model. Undoubtedly we will have to improve on several aspects of the model (the inclusion of the third spatial dimension being perhaps the most important one) before we can compare the details of the simulations with the real world. What we are showing here are minimal experiments intended to illustrate the basic mechanism — essentially to provide a schematic of the kind of development we think is taking place in the observed situation.

3. Numerical experiments

3.1. Normal-mode growth

We begin by showing the evolution of a 2000 km long baroclinic wave. We initialize the run with the "tilted sine" wave described previously, with an amplitude of 0.1 m/s for the v component. The perturbation assumes the structure of a baroclinic normal mode after an initial adjustment which we do not show. The first experiment we consider here has been run in the absence of heat fluxes (i.e., $c_E = 0$). We use this as a "reference" experiment, for comparison with the subsequent one, in which the fluxes will be active. The dashed line in Fig. 2 is the growth rate of kinetic energy of the perturbation as a function of time, after the adjustment has concluded. The growth rate is slowly declining because of non-linear equilibration of the baroclinic wave at finite amplitude, in addition to internal dissipation. Fig. 3 shows meridional wind v, vertical velocity w, potential temperature θ and mixing ratio q_v at 50 hours for this experiment.

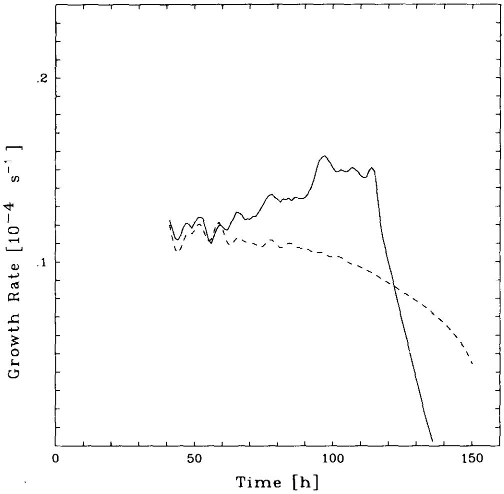

Fig. 2. Growth rate of the perturbation, in units of $10^{-4}\,s^{-1}$ vs time in hours. Solid: experiment with 2000 km domain and heat fluxes driven by a 5 K air-sea temperature difference. Dashed: same except no heat fluxes.

The zonal wind is such that the perturbation is nearly stationary. The vertical wave structure is, at this stage, that of a small amplitude baroclinic mode with a stratosphere, with maxima of v at the surface and at the tropopause. The subsequent evolution (100 h in Fig. 4 and 120 h in Fig. 5) nearly maintains the same spatial structure, with the exception of frontogenetical effects at the ground, and corresponding modifications in the vertical velocity field. It may be noted how, due to the relatively stable thermodynamic profile and low temperature, the wave's spatial structure is still closer to a dry normal mode rather than to the moist results at zero equivalent potential vorticity of Emanuel et al. (1987). Note, in particular, that the scale of the updraft exhibits little shrinking, in spite of the fact that condensation takes place (as indicated by the "noise" at low levels.)

We now repeat this experiment imposing a 5 K air-sea temperature difference. The growth rate is shown by the solid line in Fig. 2, and the area between the solid and the dashed curves can be

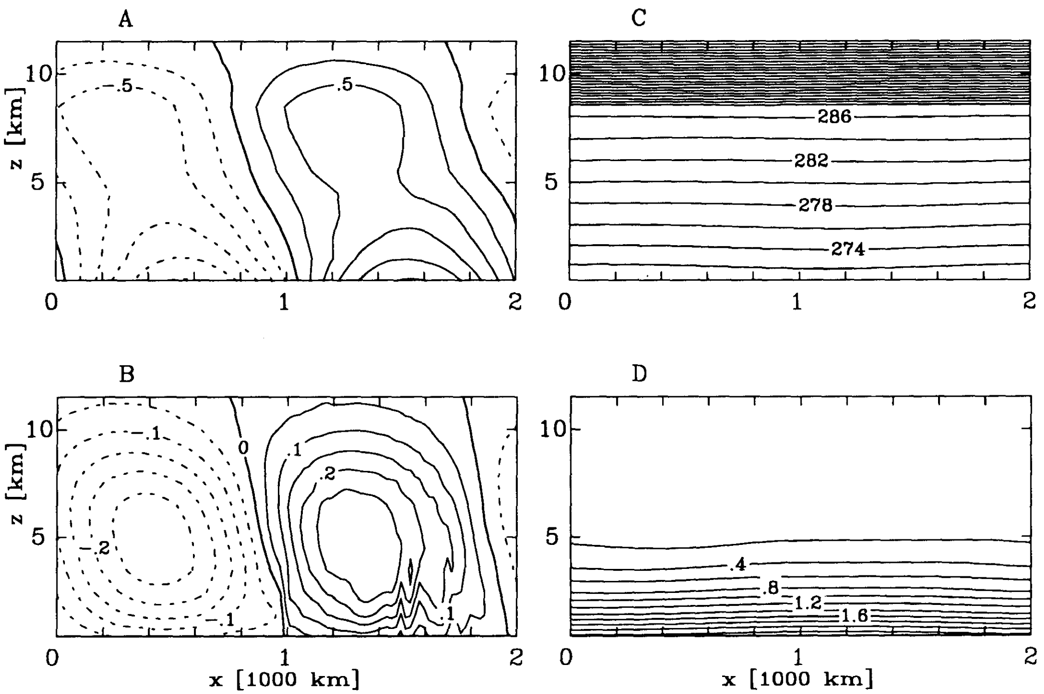

Fig. 3. Experiment with no heat fluxes (2000 km wavelength). Fields at 50 h. A: meridional wind v (m/s); B: vertical velocity w (cm/s); C: Potential temperature θ (K); D: Mixing ratio of water vapour q_v (g/kg).

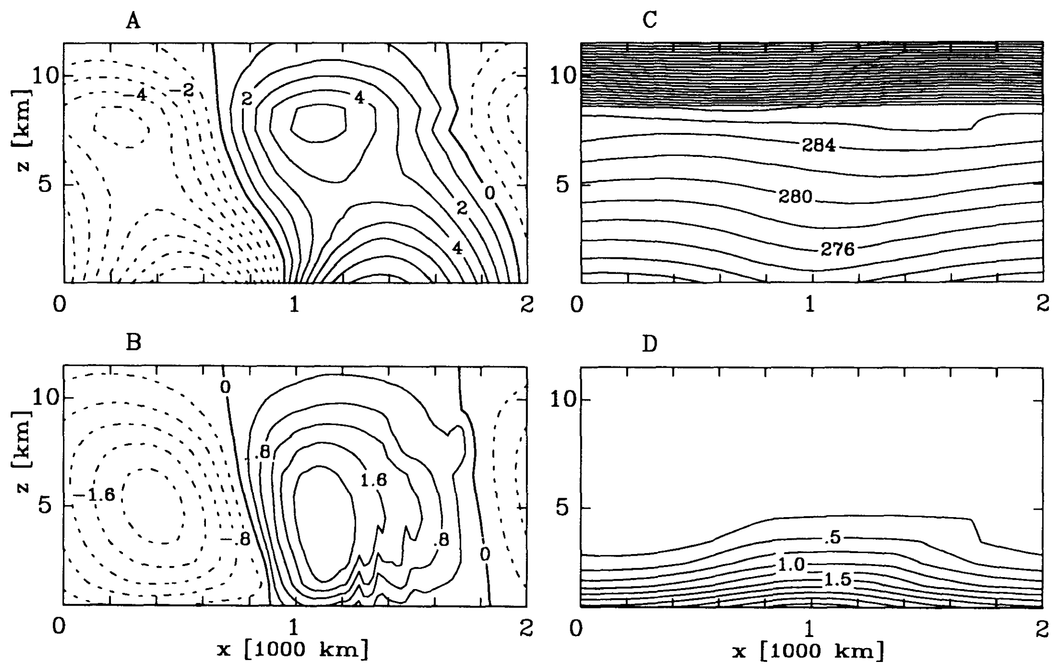

Fig. 4. Same as Fig. 3, but at 100 h.

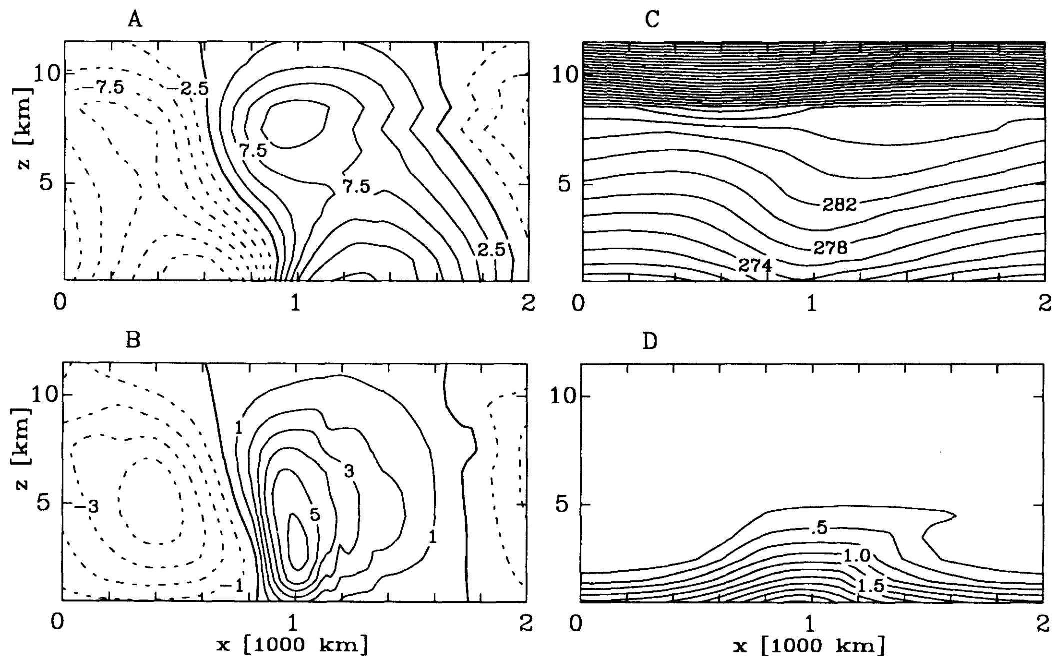

Fig. 5. Same as Fig. 3 but at 120 h.

considered as a measure of the energy the cyclone receives from the ocean. The two curves differ mainly in the interval between 90 and 120 h, indicating that, at the latter time, the fastest growing mode attains considerably larger amplitude than the mode without fluxes. The increase in growth rate is due to the emergence of a "hurricane" (convective) structure which efficiently converts the heat received at the surface into kinetic energy (see the discussion in the next session), while the sudden drop in growth rate after 120 h is due to the fact that the "hurricane" disrupts the structure of the baroclinic wave, so when the convectively induced development ceases, the perturbation is left unable to convert baroclinic APE.

We show in Fig. 6 the v field from 50 to 100 h, at intervals of 10 h, and in Fig. 7 the w field at the same times. The spatial structure of the perturbation up to 130 h (not shown) remains approximately the same as that at 100 h, with only a small widening of the updraft. The effect of the bottom fluxes on the perturbation goes from small scale convection, which is apparent in the w field but only slightly deforms the v field, to a small number (which eventually reduces to one: see Fig. 7e, f) of mesoscale updrafts, much larger than

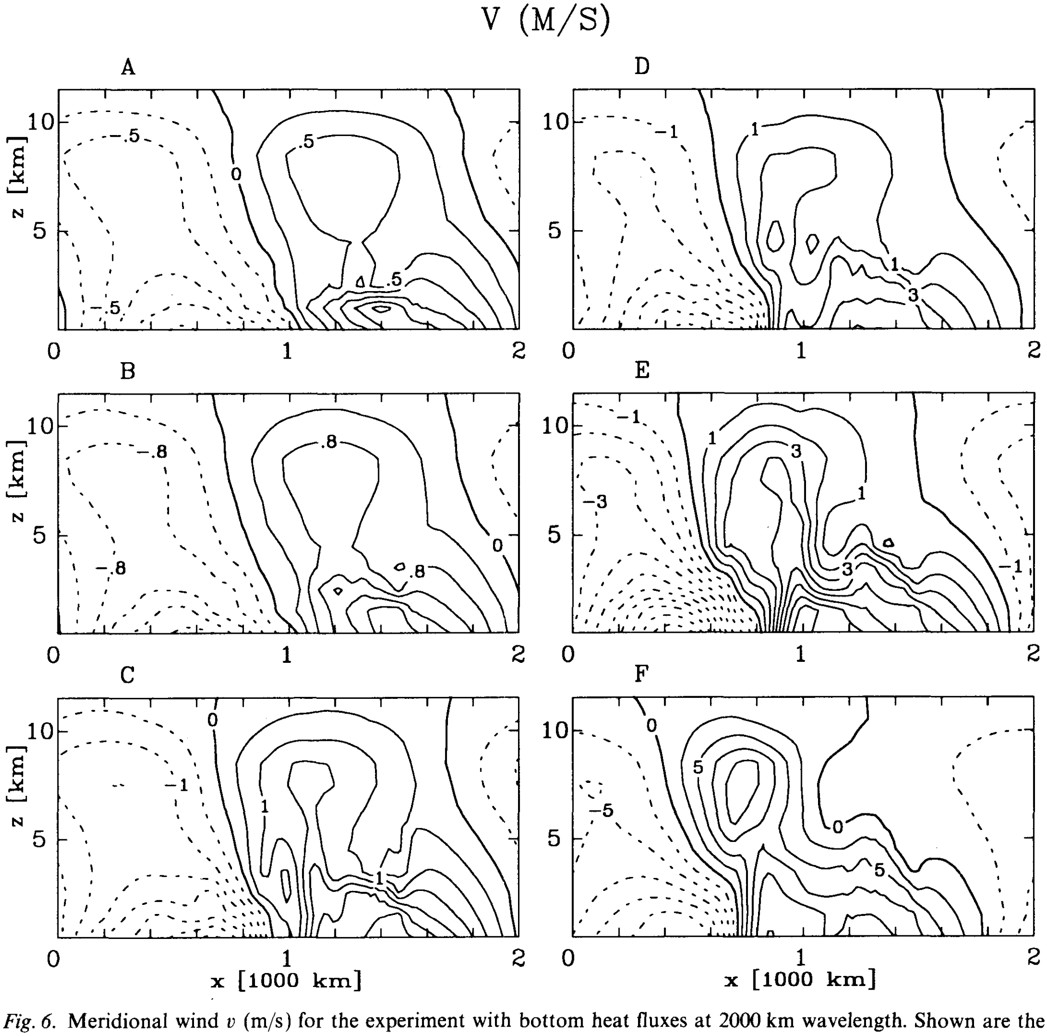

Fig. 6. Meridional wind v (m/s) for the experiment with bottom heat fluxes at 2000 km wavelength. Shown are the fields from 50 to 100 h, at 10-h interval. Contour interval changes to follow wave amplification.

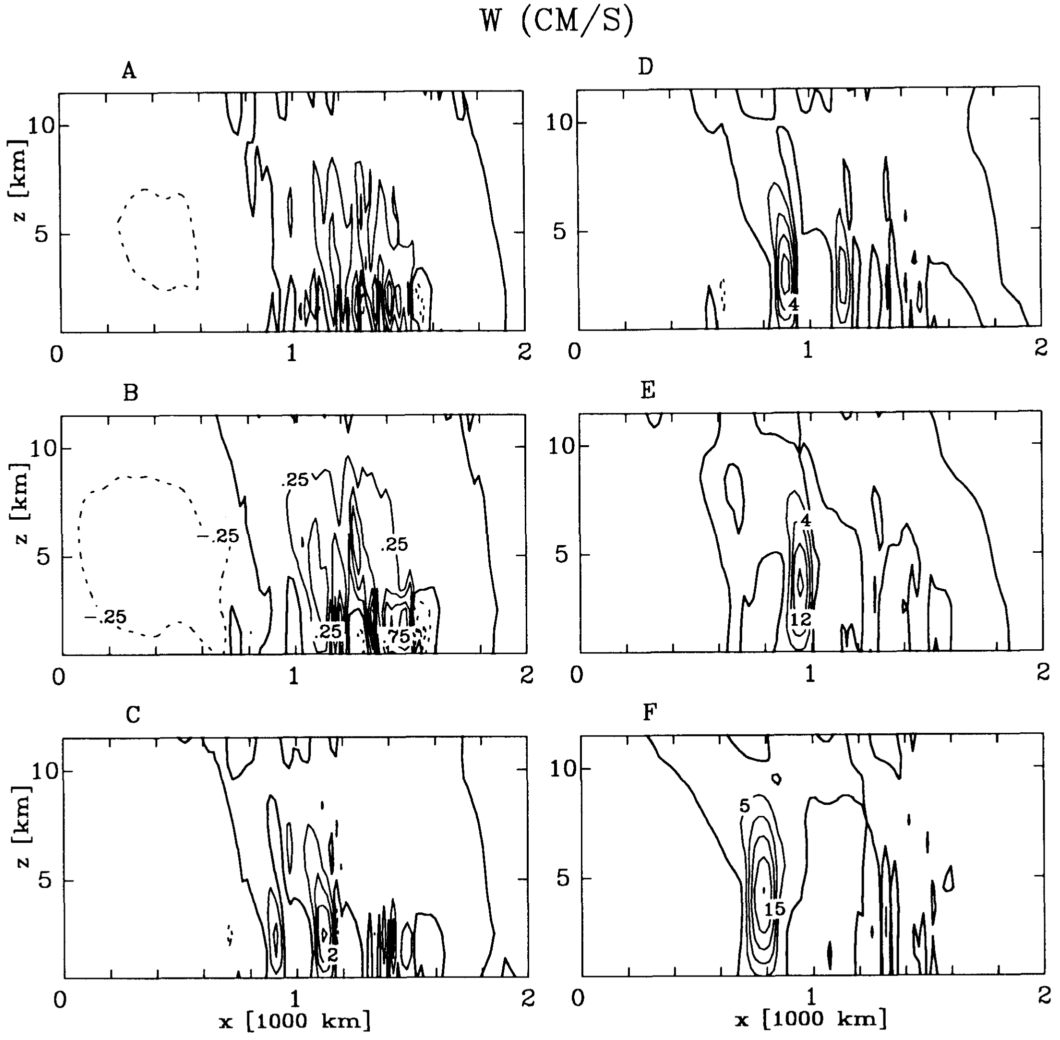

Fig. 7. Same as Fig. 6 but for vertical velocity w (cm/s).

the individual convective updrafts, and capable of significant generation of vorticity by the vortex stretching mechanism.

Fig. 8 shows the total zonal wind u and potential temperature θ at 100 hours. The total u is plotted in Fig. 8a, but only the wind perturbations associated with the components u' and v determine the bottom fluxes. The wind speed $\sqrt{u'^2+v^2}$ nearly vanishes just to the left of the base of the updraft (compare for instance Figs. 6e and 7e), while it attains the largest magnitudes on either sides.

The low level convergence in the zonal wind coincides with the location of highest potential temperature (Fig. 8b), elucidating the "warm core" nature of the system. The temperature distribution at 100 h, when compared with the initial distribution in which a 5 K air-sea temperature difference was imposed, implies that fluxes are negative at the warm core and positive elsewhere. This can be observed in Fig. 9, which shows the sensible (a) and total (sensible + latent) heat fluxes (b) at the model's lower boundary. Since the warm core near the surface almost coincides with the minimum perturbation wind speed, the negative flux of θ

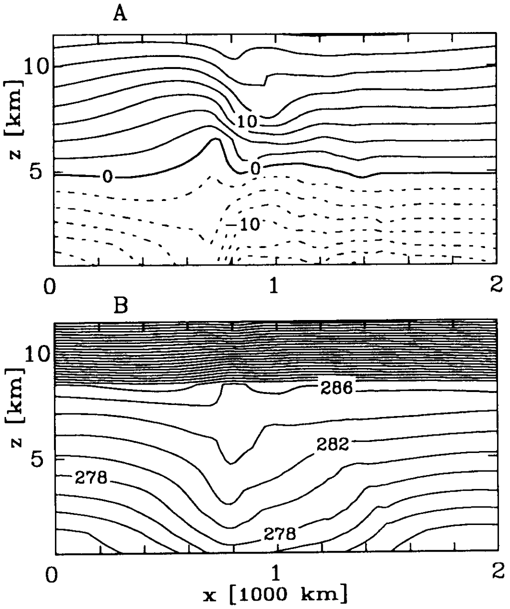

Fig. 8. Same as Fig. 6 except A: zonal wind u (m/s), at 100 h, and B: potential temperature θ (K), at 100 h.

(Fig. 9a) remains weaker than the positive flux throughout the growing stage. The sensible heat flux, integrated over the entire domain, is always positive, contributing to a general warming of the boundary layer. The predominance of positive over negative fluxes is even more evident if the total heating (sensible plus latent) is considered (Fig. 9b). Such a total flux is the most relevant for our system, since it feeds and maintains the convective updraft in the "hurricane" stage. The presence of meridional variations of temperature and moisture, associated with the baroclinic environment, seems to be important for the maintenance of an air-sea temperature contrast in the region where cold advection takes place, during the entire growth stage. The warm advection does not completely offset the effect of cold advection on the surface fluxes. The anti-correlation between advective and diabatic heating diminishes the zonal temperature contrast of the surface cold front, associated with the baroclinic growth. The convective stage does not lead, therefore, to enhanced frontogenesis.

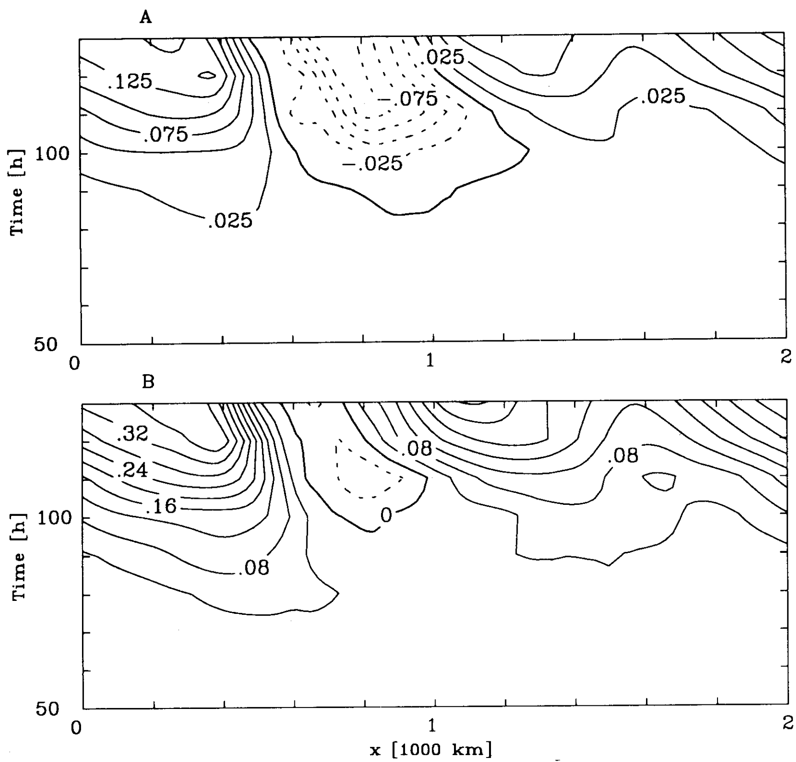

Fig. 9. $x-t$ diagrams of the fluxes of θ (A) and θ_e (B) at the lowest model level (K m/s). Same experiment as Fig. 6.

3.2. Transient growth

The experiment presented in this section is meant to represent a case departing, in the earlier phase, from the normal mode growth. In doing this, we have chosen a domain 1500 km long, so that the moist normal mode is only weakly unstable (as found numerically). In addition, we have chosen an initial perturbation similar in shape to that used in the above experiments, but with an amplitude five times larger. As a consequence, the most unstable normal mode would only become apparent near the end of the integration if no fluxes were present (not shown). What we are seeing here is a transient baroclinic growth in the early stages, from which the "hurricane" structure emerges when the convective organization prevails, with almost the same characteristics of the experiments with baroclinic modal growth.

The growth rate in this experiment (not shown) is irregular in the first 40 hours (as in the previous cases), then reaches a peak (values in excess of $0.2 \cdot 10^{-4}\,\mathrm{s}^{-1}$) at 70 h, before decaying to zero by about 110 h. Fig. 10 and 11 indicate that the mode is relatively shallow and essentially confined near the ground. Therefore, its steering level is located where the mean zonal wind is easterly. In order to better follow the evolution of the moving mode,

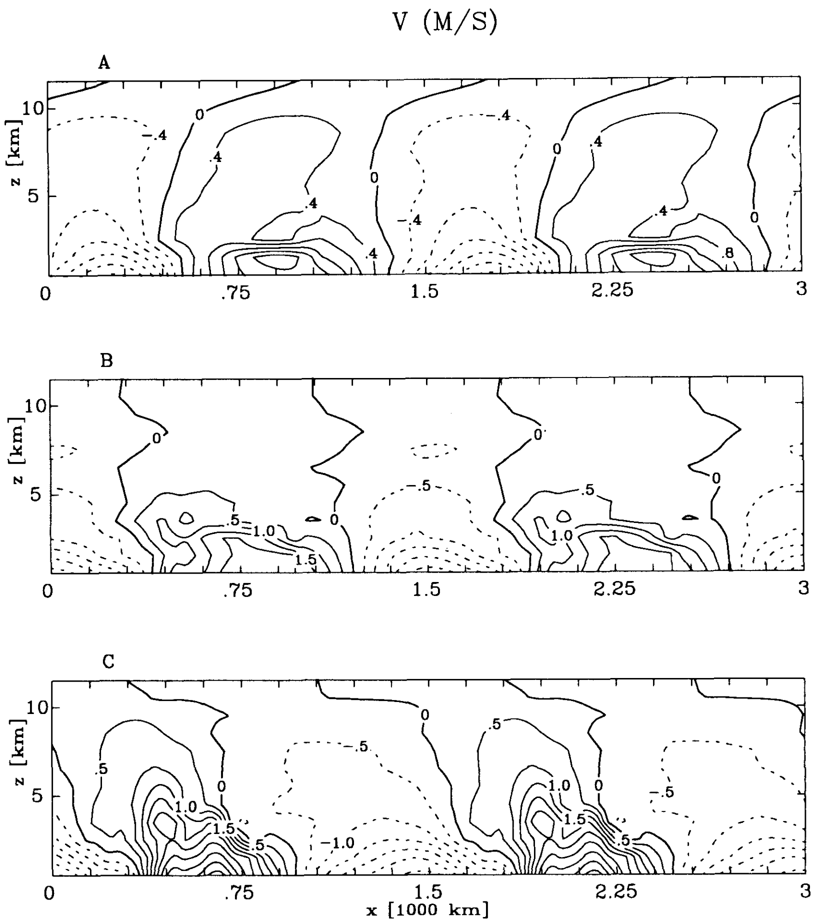

Fig. 10. Meridional wind v (m/s) for the experiment with bottom heat fluxes at 1500 km wavelength. Shown are the fields at 30, 40 and 50 h (A, B and C, respectively). The graphs show a 3000 km domain containing two wavelengths. Contour interval changes to follow wave amplification.

the figures display two wavelengths. Fig. 10 shows that the upper and lower portions of the perturbation are not locked in phase. At 30 h (Fig. 10a), the initial perturbation has assumed a reverse tilt and is unable to convert zonal APE. However, from 50 h onward (Fig. 11), when the growth rate becomes large, a consistently westward-tilted structure emerges in the v field, with the upper tropospheric portion apparently growing faster then the lower one, as demonstrated by the secondary maximum near the tropopause at 80 hours (Fig. 11c).

Fig. 12 and 13 show the corresponding evolution for the w field. By 50 h, the updraft collapses into a organized narrow structure, having the same scale as that produced in the 2000 km domain case. Note that the updraft organization is not preceded by a baroclinic modal stage, unlike the 2000 km case.

This results confirm the robustness of the "2D hurricane" like solution, that appears to be relatively independent of the initial perturbation. Such solution, therefore, does not need to arise from baroclinic instability, in the strict sense of normal mode development. However, we have not been able to obtain any similar self-sustained modes in the case of a purely barotropic environment, other basic characteristics of the initial state remaining unchanged. The strict 2D geometry of the model may well be responsible for this failure,

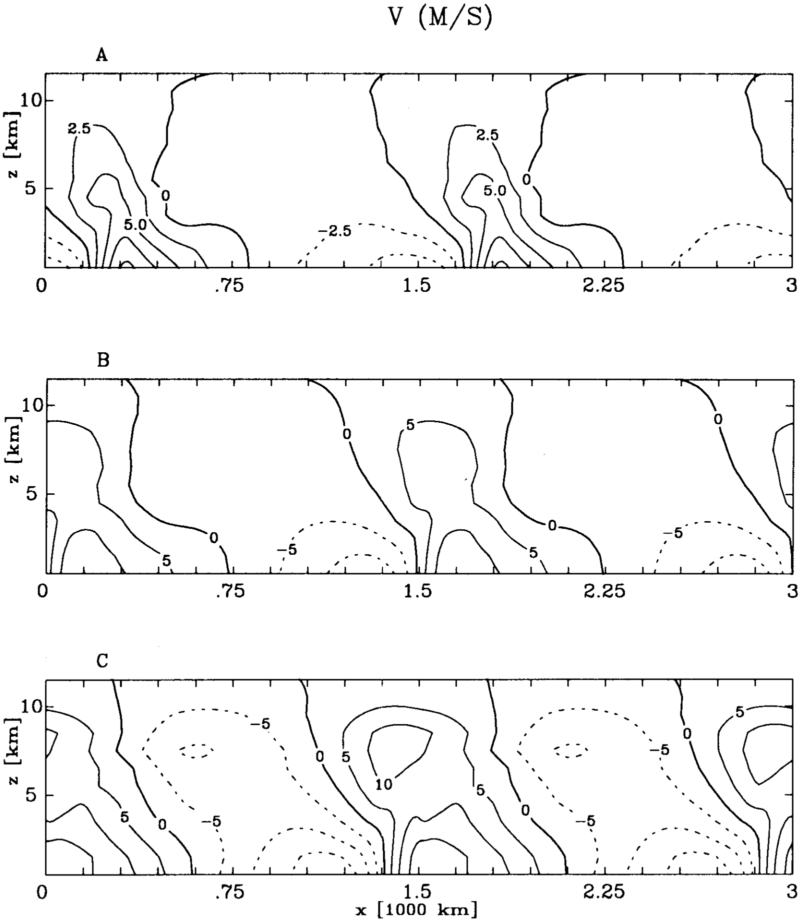

Fig. 11. Same as Fig. 9 except A: 60 h; B: 70 h; C: 80 h.

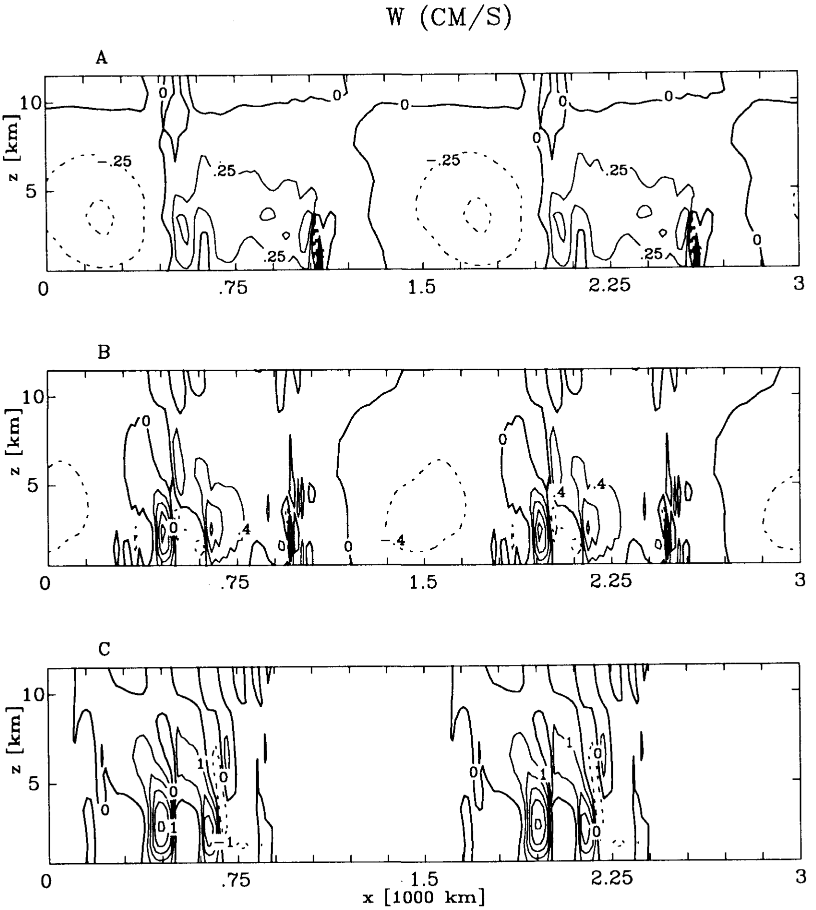

Fig. 12. Same as Fig. 9 but for vertical velocity w (cm/s).

considering that such 3D barotropic solutions have been presented in ER. In our barotropic 2D experiments, any initially imposed updraft looses coherency and soon splits into smaller scale ascent regions, unless a strong external forcing of the zonal wind is imposed.

4. Summary and conclusions

We have shown that a two-dimensional model, in which the effects of advection of moisture into the model's plane are included with the assumption of constant relative humidity in the meridional direction, is capable of representing growing modes sustained by heat fluxes from the bottom and subsequent latent heat release. Such modes have been obtained in a baroclinic atmosphere, with thermodynamic profiles and sea-air temperature contrasts typical of the polar (Antarctic, in particular) environment.

There are several similarities in the dynamical structure between the 3D barotropic case of ER and our 2D baroclinic case. In both cases, the growing stage is preceded by substantial warming and moistening of the air in the boundary layer, which is subsequently driven into an almost upright ascent region. Typical vertical velocities in the updraft are of the order of a fraction of a $m \cdot s^{-1}$, but smaller in our case than in ER. In both cases, self-sustained direct circulation, with condensation in the updraft, contributes essentially to

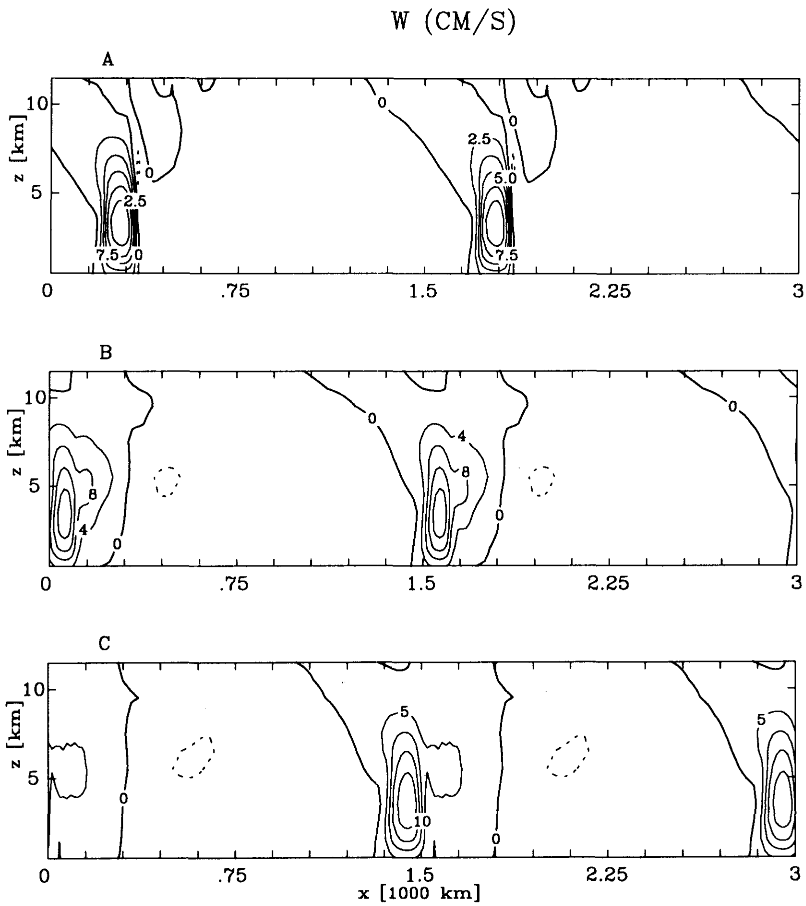

Fig. 13. Same as Fig. 11 but for 60, 70 and 80 h.

the energetics of the growing mode. There are, however, important differences between the two cases. For example, the curvature effects in the 3D case impose a gradient wind balance that implies a stronger pressure gradient for a given azimuthal (meridional, here) wind. This leads, in turn, to an adiabatic cooling of the air that converges towards the centre, thus increasing the fluxes from the sea. In addition, for reasons related to the conservation of angular momentum, wind speeds near the center of a 3D vortex are larger than those obtained in a 2D geometry. All these 3D effects cannot be present in our model. Other differences between the two cases can be ascribed mainly to the presence of the zonal vertical shear in the basic state, associated with the meridional temperature gradient. The shear affects in an essential way the vertical structure of the solution and the air motion relative to it. For example, since in our case the zonal total wind is generally much larger than the vertical velocity, trajectories cross the updraft region and do not describe a closed circulation in the vertical plane.

In the case of very small initial perturbations, our "2D polar lows" are preceded by a (moist) baroclinic stage, in which the disturbance grows to the appropriate amplitude while heat is collected from the sea and stored in the boundary layer. A distinct signature of the "hurricane" stage is given by the organization of the updraft, which contracts to a scale of the order of 100 km, smaller than the baroclinic modal scale but larger than the purely convective scale. The updraft corresponds to a warm core, where both latent heat release and horizontal advection contribute to local heating. We have been able to obtain a similar flow organization, with almost the same spatial scales, also in the case of a non modal initial stage. This fact implies that the initial growth related to baroclinic instability is not essential for the organization of the finite-amplitude circulation.

The main reasons for our insisting that these are not just ordinary moist baroclinic normal modes (as those illustrated in our Figs. 3–5, and, e.g., in Fig. 9a of Joly and Thorpe, 1989), despite the similarities in the vertical and horizontal wind structure, are: (i) the strong, vertically coherent, "warm core" thermal perturbation (see Fig. 8b) and (ii) the independence of the horizontal scale of the convective stage from the wavelength of the initial baroclinic perturbation. In our opinion these two points, and the peak in growth rate that accompanies them, strongly hint at an "individuality" of the convective stage, distinct from baroclinic modes.

The importance of the baroclinicity is probably related not so much to the baroclinic instability potential as to the presence of meridional gradients of temperature and moisture, that allow substantial variations of these quantities in the model plane, via meridional advection. In fact, the warming and moistening of the lowest layers by the air-sea exchange predominates during the growth stage. The zonal wind component carries the warm and moist air into the updraft. Such advection is not symmetric around the updraft, in contrast with the barotropic case.

We have tried to verify the importance of baroclinicity by running an experiment in which the shear of the basic zonal wind and the meridional gradients of thermodynamic quantities were gradually removed after the development of the convective stage (90 h in Fig. 6). This procedure introduces spurious accelerations that make the zonal wind component oscillate widely. It becomes clear, however, from the temperature field (not shown) that the absence of meridional advection quickly destroys the warm core structure and the associated circulation, including the coherent updraft. It seems, at this point, that the maintenance of air-sea temperature difference is crucial for the survival of the 2D convective stage. We cannot exclude that in 3D barotropic cases the air-sea contrast could be maintained by other mechanisms. We already mentioned the adiabatic cooling of air moving radially inward. Moreover, the ratio between the cooler region in which heat is fed into the air and the central warm region is much larger, for purely geometrical reasons, in the 3D case. Finally, in some real cases of polar lows the initial air-sea temperature difference can be larger than here assumed. In contrast to tropical environments, where the air-sea exchange is mostly in the form of latent heat, and does not warm the boundary layer, the maintenance of a temperature difference, and thus of sensible heat influx, would be crucial for a polar low.

5. Acknowledgements

We wish to thank Professor A. J. Thorpe for his helpful comments. This work was supported by the "Progetto Nazionale di Ricerche in Antartide". Preliminary results were presented at the workshops "Italian Research on Antarctic Atmosphere" in 1990 and 1991 and appeared in the Proceedings of those meetings.

REFERENCES

Bromwich, D. H. 1989. Sub-synoptic scale cyclone developments in the Ross Sea sector of the Antarctic. *Polar and Arctic Lows*. A. Deepak Publishing, 421 pp.

Carleton, A. M. and Carpenter, D. A. 1989. Satellite climatology of "polar air" vortices for the southern hemisphere winter. *Polar and Arctic Lows*. A. Deepak Publishing, 421 pp.

Emanuel, K. A. 1986. An air-sea interaction theory for tropical cyclones. Part I: Steady state maintenance. *J. Atmos. Sci. 43*, 585–604.

Emanuel, K., Fantini, M. and Thorpe, A. J. 1987. Baroclinic instability in an environment of small stability to slantwise moist convection. Part I: two-dimensional models. *J. Atmos. Sci. 44*, 1559–1573.

Emanuel, K. A. and Rotunno, R. 1989. Polar lows as Arctic hurricanes. *Tellus 41A*, 1–17.

Fantini, M. 1990. The effect of heat and moisture fluxes from the ocean on the development of baroclinic waves. *J. Atmos. Sci. 47*, 840–855.

Fantini, M. 1993. A numerical study of 2D moist baroclinic instability. *J. Atmos. Sci.*, in press.

Fitch, M. and Carleton, A. M. 1992. Antarctic mesocyclone regimes from satellite and conventional data. *Tellus 44A*, 180–196.

Heinemann, G. 1990. Mesoscale vortices in the Weddell Sea Region (Antarctica). *Mon. Wea. Rev. 118*, 779–793.

Hoskins, B. J., Hsu, H. H., James, I. N., Masutani, M., Sardeshmukh, P. D. and White, G. H. 1989. Diagnostics of the Global Atmospheric Circulation, based on ECMWF analyses 1979–1989. *World Climate Programme Research*, no. 27. WMO.

Joly, A. and A. J. Thorpe, 1989. Warm and occluded fronts in two-dimensional moist baroclinic instability. *Quart. J. Roy. Meteor. Soc. 115*, 513–534.

Klemp, J. B. and Wilhelmson, R. B. 1978. The simulation of three dimensional convective storm dynamics. *J. Atmos. Sci. 35*, 1070–1096.

Mansfield, D. A. 1974. Polar lows: The development of baroclinic disturbances in cold air outbreaks. *Quart. J. Roy. Meteor. Soc. 100*, 541–554.

Rasmussen, E. A. 1985. A case study of polar low development over the Barents Sea. *Tellus 37A*, 407–418.

Rasmussen, E. A., Pedersen, T. S., Pedersen, L. T. and Turner, J. 1992. Polar lows and arctic instability lows in the Bear Island region. *Tellus 44A*, 133–154.

Rotunno, R. and Emanuel, K. A. 1987. An air-sea interaction theory for tropical cyclones. Part II: Evolutionary study using a nonhydrostatic axisymmetric numerical model. *J. Atmos. Sci. 44*, 542–561.

Sardie, J. M. and Warner, T. T. 1983. On the mechanism for the development of polar lows. *J. Atmos. Sci. 40*, 869–881.

Wiin-Nielsen, A. 1989. On the precursors of polar lows. *Polar and Arctic Lows*. A. Deepak Publishing, 421 pp.

Tellus A/45/2-3